

ORIGINAL ARTICLE

CHCHD10 mutations p.R15L and p.G66V cause motoneuron disease by haploinsufficiency

Sarah J. Brockmann¹, Axel Freischmidt¹, Patrick Oeckl¹, Kathrin Müller¹, Srinivas K. Ponna², Anika M. Helferich¹, Christoph Paone³, Jörg Reinders⁴, Kerstin Kojer¹, Michael Orth¹, Manu Jokela⁵, Mari Auranen⁶, Bjarne Udd⁵, Andreas Hermann^{7,8,9}, Karin M. Danzer¹, Peter Lichtner¹⁰, Paul Walther¹¹, Albert C. Ludolph¹, Peter M. Andersen¹², Markus Otto¹, Petri Kursula^{2,13}, Steffen Just³ and Jochen H. Weishaupt^{1,*}

¹Department of Neurology, Ulm University, 89081 Ulm, Germany, ²Faculty of Biochemistry and Molecular Medicine, University of Oulu, 90014 Oulu, Finland, ³Molecular Cardiology, Department of Internal Medicine II, Ulm University Medical Center, 89081 Ulm, Germany, ⁴Institute for Functional Genomics, University Regensburg, 93053 Regensburg, Germany, ⁵Neuromuscular Research Center, Tampere University and University Hospital, 33014 Tampere, Finland, ⁶Neurological Department, Helsinki University Hospital, 00029 Helsinki, Finland, ⁷Department of Neurology, Technische Universität Dresden, 01307 Dresden, Germany, ⁸German Center for Neurodegenerative Diseases, Dresden Research Site, 01307 Dresden, Germany, ⁹Center for Regenerative Therapies Dresden (CRTD), Technische Universität Dresden, 01307 Dresden, Germany, ¹⁰Institute of Human Genetics, Helmholtz Zentrum München, 85764 Neuherberg, Germany, ¹¹Zentrale Einrichtung Elektronenmikroskopie, Universität Ulm, 89081 Ulm, Germany, ¹²Department of Pharmacology and Clinical Neuroscience, Umeå University, 90187 Umeå, Sweden and ¹³Department of Biomedicine, University of Bergen, 5020 Bergen, Norway

*To whom correspondence should be addressed at: Ulm University, Department of Neurology, Albert-Einstein-Allee 11, 89081 Ulm, Germany. Tel: +49 73150063073; Fax: +49 73150063050; Email: jochen.weishaupt@uni-ulm.de

Abstract

Mutations in the mitochondrially located protein CHCHD10 cause motoneuron disease by an unknown mechanism. In this study, we investigate the mutations p.R15L and p.G66V in comparison to wild-type CHCHD10 and the non-pathogenic variant p.P34S *in vitro*, in patient cells as well as in the vertebrate *in vivo* model zebrafish. We demonstrate a reduction of CHCHD10 protein levels in p.R15L and p.G66V mutant patient cells to approximately 50%. Quantitative real-time PCR revealed that expression of CHCHD10 p.R15L, but not of CHCHD10 p.G66V, is already abrogated at the mRNA level. Altered secondary structure and rapid protein degradation are observed with regard to the CHCHD10 p.G66V mutant. In contrast, no significant differences in expression, degradation rate or secondary structure of non-pathogenic CHCHD10 p.P34S are detected when compared with wild-type protein. Knockdown of CHCHD10 expression in zebrafish to about 50% causes motoneuron pathology, abnormal myofibrillar structure and motility deficits *in vivo*. Thus, our data show that the CHCHD10 mutations p.R15L and p.G66V cause motoneuron disease primarily based on haploinsufficiency of CHCHD10.

Received: October 17, 2017. Revised: December 8, 2017. Accepted: December 18, 2017

© The Author(s) 2018. Published by Oxford University Press. All rights reserved.

For Permissions, please email: journals.permissions@oup.com

Introduction

Impairment of mitochondria has repeatedly been suggested to contribute to the pathogenesis of amyotrophic lateral sclerosis (ALS) (1,2). However, the observed mitochondrial alterations may be secondary events, and genetic support for mitochondrial dysfunction as a primary cause of motoneuron degeneration was still lacking. However, recently, rare missense mutations in the coiled-coil-helix-coiled-coil-helix domain containing protein 10 (CHCHD10) were linked to a diverse disease spectrum including myopathy, cerebellar ataxia, frontotemporal dementia (FTD) (3) as well as motoneuron diseases (MND), specifically ALS (3,4) and spinal muscular atrophy Jokela type (SMAJ) (5,6).

CHCHD10 is a nuclear gene, but expression of its protein product is mainly limited to mitochondria (3). CHCHD10 is part of the mitochondrial contact site and cristae organizing system (MICOS) complex at the inner mitochondrial membrane (7). No major mitochondrial structural changes were observed in SMAJ muscle tissue (8) while it has been shown that ALS- and FTD-causing CHCHD10 mutations lead to structural and functional impairments of mitochondria (3,7). Therefore, CHCHD10 mutations could provide the first human genetic evidence that primary mitochondrial damage can cause MND. However, it remained largely unclear whether motoneuron disease-causing mutations in CHCHD10 lead to a loss of physiological function, a dominant-negative effect as suggested by very recent work (9) or novel toxic properties completely unrelated to its physiological role. Distinguishing between these possibilities is central to the understanding of CHCHD10-related neurodegeneration and the role of mitochondrial damage in motoneuron diseases. Respective insights have also been hampered by the lack of biomaterial from a sufficient number of rare CHCHD10 mutation carriers and the predominant use of overexpression models (3,7,9).

In this study, we use cell lines of a total of 13 patients to show that the CHCHD10 mutations p.R15L and p.G66V cause MND by reduced expression of the mutant protein and haploinsufficiency of CHCHD10. We furthermore corroborate our findings by biochemical assays and an *in vivo* zebrafish model.

Results

The subsequent studies are based on the two motoneuron disease-associated CHCHD10 mutations with the strongest evidence for causality: CHCHD10^{G66V} is a rare variant which has been shown to co-segregate with a lower motoneuron syndrome in 17 Finnish families (5) and was found in one familial index patient (4). CHCHD10^{R15L} is another rare variant that has been detected in three German families (4,10) as well as three ALS families in the United States (11). As a control condition in addition to wild-type (WT) CHCHD10 we used CHCHD10^{P34S}. The p.P34S variant of CHCHD10 represents a polymorphism with a frequency of overall 0.6% in control populations and has been shown not to be associated with ALS in multiple studies (12,13).

p.R15L and p.G66V mutations lead to reduced CHCHD10 protein levels in patient-derived cells

Western blot analysis of ALS patient-derived lymphoblastoid cell lines (LCLs) and primary fibroblasts carrying the CHCHD10 p.R15L and p.G66V mutation, respectively, revealed an approximately 50% reduction in protein levels compared with healthy controls (Fig. 1A, Supplementary Material, Fig. S1). The total amount of

mitochondria was not affected in patient cells as suggested by Western blotting of the mitochondrial marker HSP60 (Fig. 1B, Supplementary Material, Fig. S1) and quantitative real-time PCR (qRT-PCR) of four mitochondrially encoded genes (Fig. 1C). Additionally, transmission electron microscopy (TEM) did not reveal altered mitochondrial ultrastructure in patient-derived cells (Fig. 1D). qRT-PCR demonstrated a reduction of CHCHD10 mRNA to approximately 50% in the heterozygous CHCHD10^{R15L} mutant patient cells (Fig. 1E). Subsequent sequencing of the respective cDNA revealed a complete loss of CHCHD10^{R15L} mutated mRNA, while expression of the WT allele was confirmed (Fig. 1F). LCLs carrying the p.P34S variant, which is not associated with ALS, did not reveal any changes of CHCHD10 mRNA or protein expression, and sequencing of the CHCHD10 cDNA indicated similar expression of both alleles.

In fibroblasts of CHCHD10^{G66V} mutation carriers, TDP-43 staining did not reveal a nucleocytoplasmic translocation of TDP-43 (at least 100 cells analysed per condition), which contrasts with results from a previous report based on CHCHD10 knockdown in primary mouse neurons and murine neuronal NIH3T3 cells (9). Additionally, we could not detect any accumulation of cytoplasmic stress granules, as judged by staining of TIAR (Fig. 1G).

CHCHD10 p.G66V shows an increased degradation rate

We found that both mutations, CHCHD10^{R15L} and CHCHD10^{G66V}, lead to an approximately 50% decrease in CHCHD10 protein level. In contrast to CHCHD10^{R15L}, CHCHD10^{G66V} mRNA was normally expressed. Therefore, we hypothesized that the reduction in CHCHD10^{G66V} protein was the result of instability and increased degradation on the protein level. Consequently, we performed a pulse-chase experiment in HEK293 cells overexpressing CHCHD10 for 24 h, followed by cycloheximide (CHX, 30 µg/ml) treatment to inhibit protein translation for up to 6 h (Fig. 2A). Subsequent quantitative analysis of the CHCHD10 protein level by Western blotting showed substantially increased degradation rates of CHCHD10^{G66V} compared with CHCHD10^{WT} and CHCHD10^{P34S} after 6 h of CHX treatment (Fig. 2B). In addition, CHCHD10^{R15L} protein displayed a trend towards faster degradation. Next, we employed circular dichroism spectroscopy to study recombinant CHCHD10 protein (Fig. 2C). Overall, the spectra had expected shapes, considering that the predicted structure of CHCHD10 consists of long disordered regions and three α -helices. After addition of 0.1% DPC, mimicking membrane conditions, both CHCHD10^{R15L} and CHCHD10^{G66V} showed distinct structural differences with an increased α -helical content when compared with CHCHD10^{WT} and the non-pathogenic CHCHD10^{P34S} variant (Fig. 2D). This suggests that improper protein folding may induce an increased degradation rate of CHCHD10 pathogenic variants. The fact that these differences are pronounced under membrane-mimicking conditions can be explained by the fact that CHCHD10^{R15L} and CHCHD10^{G66V} are both more hydrophobic than CHCHD10^{WT}.

In vivo knockdown of CHCHD10 in zebrafish leads to neuronal and muscular pathology as well as impaired locomotion

As our data obtained from patient-derived cells and biochemical experiments suggested haploinsufficiency of CHCHD10 protein as the predominant pathogenic consequence of CHCHD10^{G66V} and CHCHD10^{R15L} mutations, we next aimed to validate this molecular genetic mechanism *in vivo*. Accordingly, we induced a

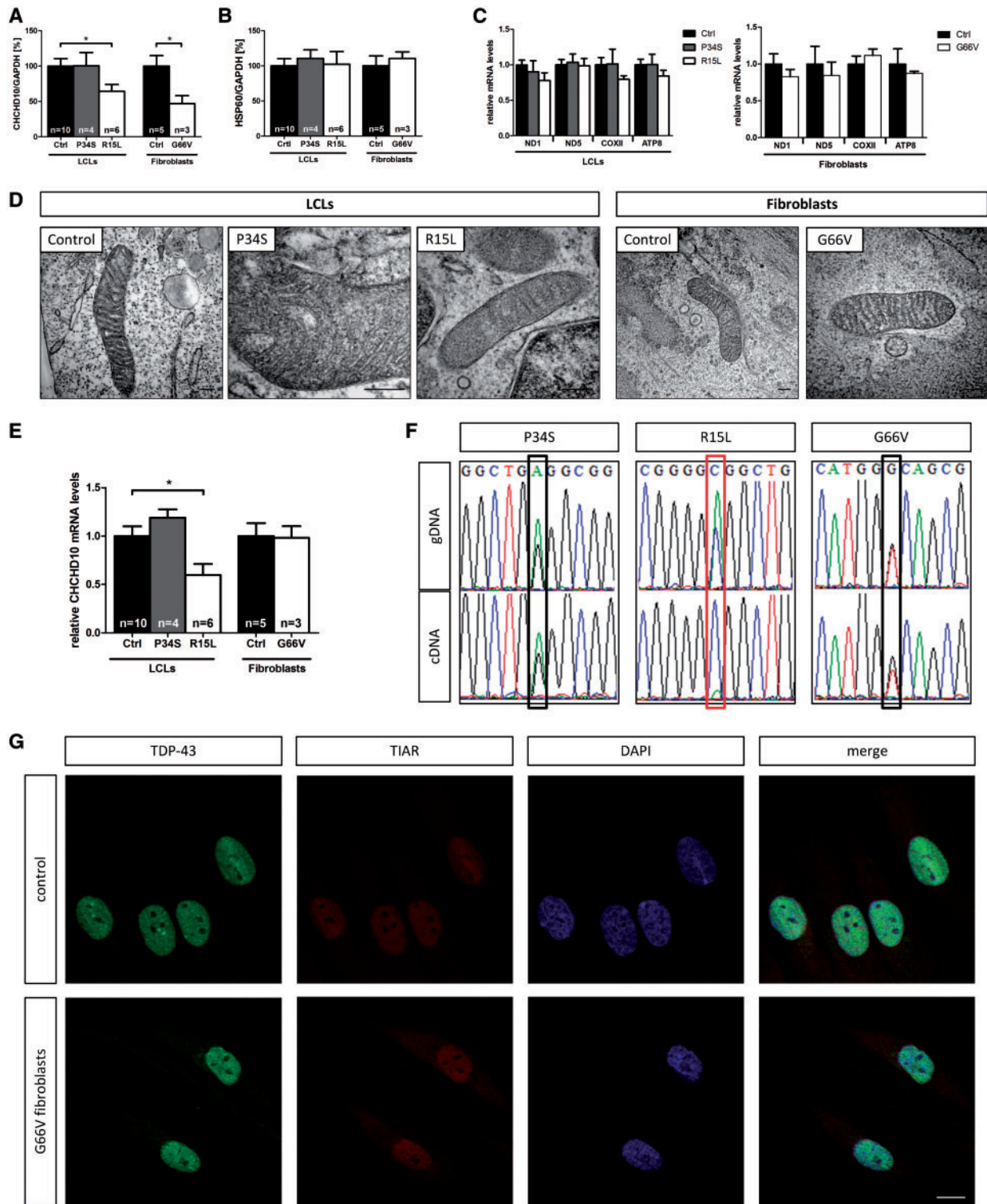


Figure 1. CHCHD10 protein and/or mRNA levels are reduced in patient-derived cells. (A) Densitometric analysis of Western blots comparing CHCHD10 levels of LCLs carrying a CHCHD10^{P34S} variant (n = 4) or CHCHD10^{R15L} mutation (n = 6) with ten healthy controls, and of fibroblasts carrying a CHCHD10^{G66V} mutation (n = 3) with fibroblasts from five healthy controls. Western blots were performed in triplicates. (B) Densitometric quantification of Western blots comparing relative levels of mitochondrial marker HSP60 of LCLs from four CHCHD10^{P34S} and six CHCHD10^{R15L} mutation carriers to ten healthy controls as well as of fibroblasts from three CHCHD10^{G66V} mutation carriers to five healthy controls. (C) Relative mRNA levels of mitochondrially encoded genes in the same cell lines as used for Western blotting in (A) and (B). Ct-values were normalized to TBP. (D) Representative transmission electron microscopic images of mitochondrial ultrastructure in patient derived cells (Scale bars indicate 200 nm). (E) Relative CHCHD10-mRNA levels as determined by qRT-PCR in the same cell lines from patients and control individuals used before. Ct-values were normalized to TBP. (F) Sequencing results of CHCHD10 genomic DNA (gDNA) and cDNA of patient-derived cell lines. Note the absence of the mutated allele in the cDNA from cells carrying the p.R15L mutation. (G) TDP-43 localization in fibroblasts of CHCHD10^{G66V} mutation carriers. Staining of TIAR was used to detect possible stress granule formation (Scale bar indicates 10 μm). [Bars in (A), (B) and (E) indicate mean ± s.e.m.; *P < 0.05 in a two-tailed student's t-test].

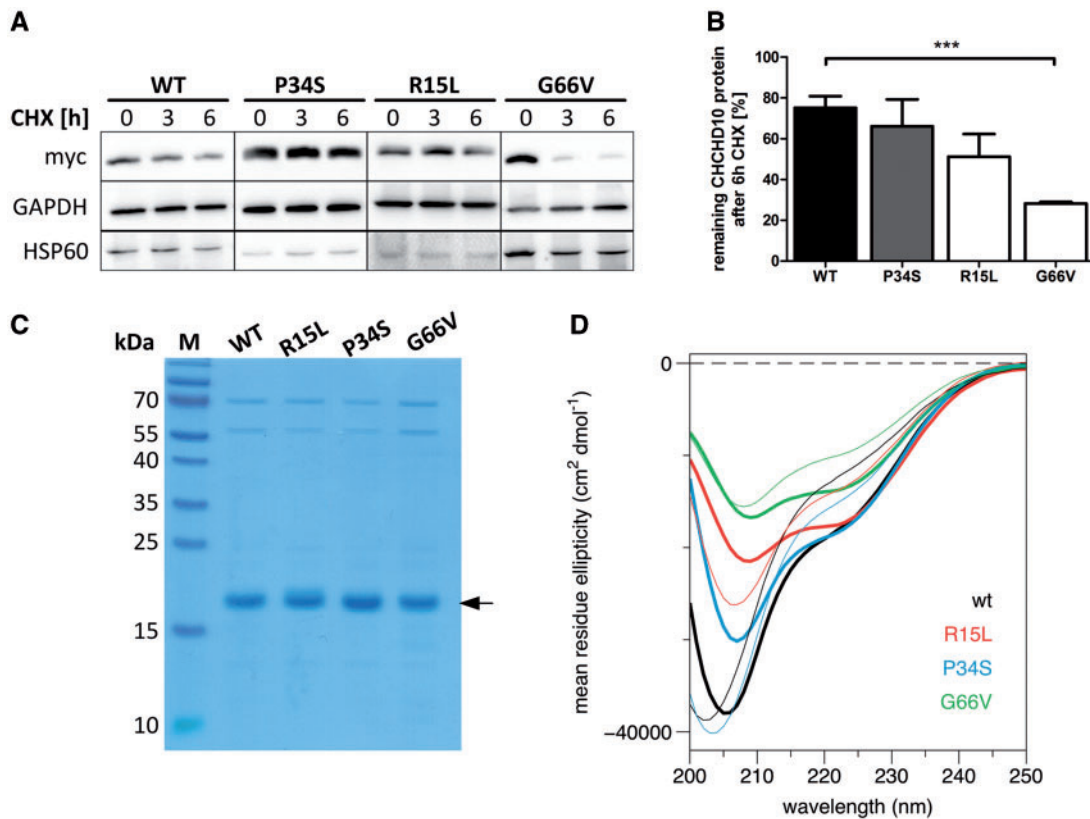


Figure 2. CHCHD10^{G66V} shows an increased protein degradation rate and structural alterations. (A) HEK293 cells overexpressing WT or mutant CHCHD10-myc for 24 h were treated with cycloheximide (CHX; 30 μ g/ml) to inhibit protein translation. Cells were harvested and subjected to Western blotting at the indicated time points. Representative Western blots of five independent experiments are shown. (B) Densitometric analysis of Western blots ($n = 5$) shown in (A) after 6 h of CHX treatment compared with starting point. (Bars represent mean \pm s.e.m.; *** $P \leq 0.001$ in a two-tailed student's t -test) (C) Coomassie-stained SDS-gel of recombinant CHCHD10 variants purified from *E. coli* and used for CD spectroscopy. (D) CD spectra of purified CHCHD10 proteins. Spectra were acquired in PBS with 0.02% (thin lines) and 0.1% (thick lines) dodecylphosphocholine (DPC). The higher concentration, being above the critical micellar concentration, mimics membrane conditions. The spectra of CHCHD10^{WT} and CHCHD10^{P34S} are similar whereas the spectra of CHCHD10^{R15L} and CHCHD10^{G66V} show an increased α -helical content, especially at 0.1% DPC.

transient knockdown in zebrafish embryos using two different morpholinos directed against the translation initiation site (MO1) or a splice site (MO2, exon1-intron1) of CHCHD10 pre-mRNA. A standard control morpholino (CoMO) served as injection control. Human and zebrafish CHCHD10 share about 66% sequence identity at the protein level with a high conservation of the characteristic hydrophobic helix and the C-terminal CHCH-domain (Fig. 3A). Confirmation of CHCHD10 knockdown to approximately 50% by both morpholinos at 48 hours post fertilization (hpf) was based on mass spectrometric analysis (Fig. 3B), as no antibody directed against *Danio rerio* CHCHD10 orthologue was available. We thus achieved a degree of CHCHD10 protein knockdown that resembles the situation in human CHCHD10 mutant cells. The CHCHD10 knockdown did not alter gross morphology of the fish except for an unspecific heart edema that is most likely caused by the injection procedure since it is also observed in control morpholino-injected embryos (Fig. 3C). However, in an unbiased hierarchical cluster analysis of the proteomic profiles obtained from zebrafish embryos that were injected with MO1, MO2, CoMO or remained uninjected, biological replicates from each condition clustered together, suggesting that the different treatments resulted in distinct but consistent alterations of the proteome (Fig. 3D). Non-injected and CoMO-injected controls, as well as MO1- and MO2-injected embryos clustered together, respectively, indicating similar alterations of the proteome by CHCHD10 knockdown

irrespective of the morpholino used, and little changes caused by the control morpholino.

Furthermore, both MO1- and MO2-mediated knockdown of CHCHD10 led to a similar pathology: Both morphants showed motoneuron pathology with significantly reduced axon lengths (Fig. 3E). Moreover, MO1- as well as MO2-injection led to a significant reduction of light polarization by myofibrils, indicating a disturbance of the normally highly ordered structure of the zebrafish skeletal muscle [Fig. 4A (upper panel) and B]. This finding was corroborated by electron microscopy [Fig. 4A (middle panel)] and a gene ontology analysis of the proteomic data. Downregulated proteins of both, MO1- and MO2-injected embryos, were highly significantly enriched for proteins located in myofibers and other muscle-specific structures (Supplementary Material, Table S2). Mitochondrial ultrastructure in muscle tissue appeared normal as shown in TEM images in Figure 4A (lower panel). Thus, our zebrafish CHCHD10 knockdown model is reminiscent of both the neuronal and myopathic phenotypes observed in MND patients carrying a CHCHD10 mutation.

The observed cellular abnormalities resulted in functional deficits. CHCHD10 knockdown embryos showed a decrease in the touch-induced flight response (Fig. 4C, Supplementary Materials, Videos). Both, the functional and the above described neuromuscular phenotype, could be rescued by co-injection of morpholino with CHCHD10 mRNA (Supplementary

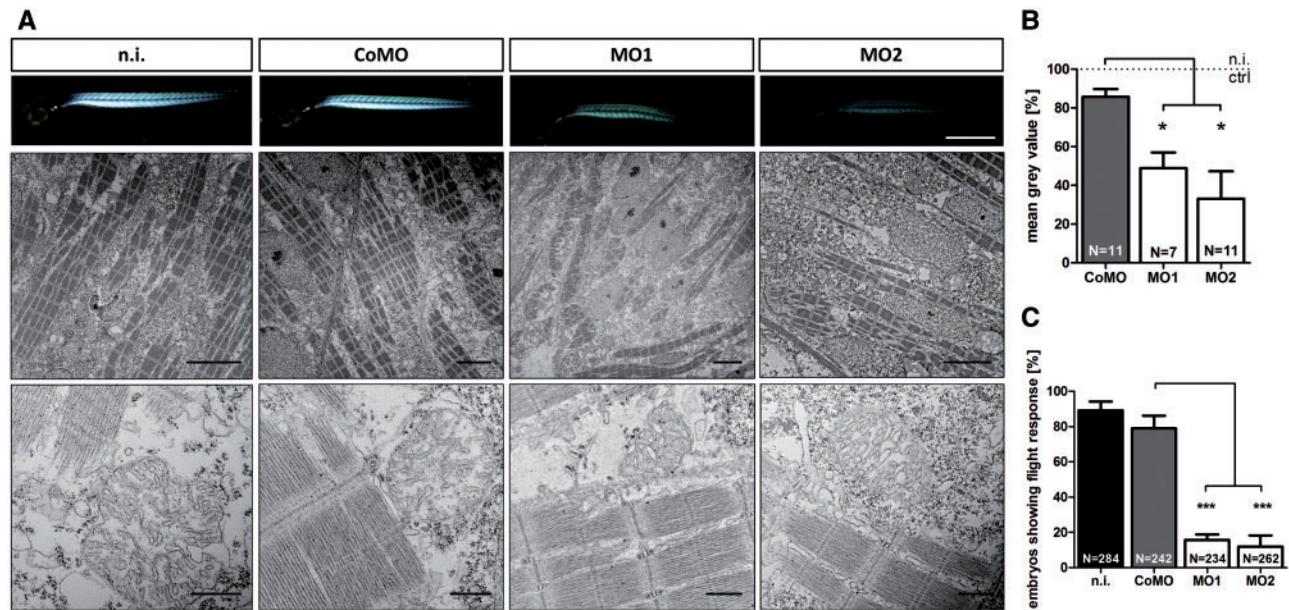


Figure 4. CHCHD10 knockdown embryos exhibit altered myofibrillar structure and a motility phenotype. (A, upper panel) Birefringence of 72 hpf old embryos. Bright birefringence signals are caused by polarization of light of highly ordered myofibrillar structures (Scale bar indicates 500 μ m). (A, middle panel) Transmission electron microscopy (TEM) of muscle tissue of zebrafish embryos (48 hpf) (Scale bars indicate 5 μ m). (A, lower panel) TEM images of mitochondria in muscle tissue of zebrafish embryos (48 hpf) (Scale bars indicate 500 nm). (B) Quantification of the birefringence signals shown in (A) using Image J software. Birefringence signals of the non-injected control were set to 100% ($n=3$ independent experiments). (C) Touch-induced flight response of CHCHD10 knockdown embryos 48 hpf. Co-injection of MO2 and CHCHD10 mRNA rescued the motility phenotype observed with MO1 or MO2 injection only ($n=3-4$ independent experiments; n indicates the total number of embryos analysed; bars indicate mean \pm s.e.m.; * $P \leq 0.05$, *** $P \leq 0.001$ in a two-tailed student's t-test; n.i. = non-injected control).

detect a significant enrichment of p.P34S in ALS patients when compared with healthy controls, arguing against a pathogenic role (12,13).

A most recent study (9) suggests that two CHCHD10 mutations, including p.S59L as well as the p.R15L mutation studied in this work, result in impairment of mitochondrial integrity besides reduction in synapse numbers as well as in accumulation of cytoplasmic TDP-43. The authors propose that CHCHD10 mutations act by loss of function or a dominant negative principle. However, Woo *et al.* do not present CHCHD10 expression data from patient material and heavily rely on overexpression models. In contrast, our results demonstrating loss of expression of CHCHD10 mutant alleles are based on a total of 13 patient cell lines and three different CHCHD10 variants in addition to cell lines from healthy control individuals. In our patient-derived cell lines we could neither observe an alteration of mitochondrial ultrastructure, nor the TDP-43 mislocalization previously reported by Woo *et al.* upon CHCHD10 knockdown. Of note, during the revision of this manuscript, a parallel publication (15) also reported a normal mitochondrial morphology in patient fibroblasts carrying the CHCHD10 p.R15L mutation. Nevertheless, the detrimental effects of shRNA-mediated CHCHD10 knockdown *in vitro* and knockout of the CHCHD10 orthologue in *C. elegans* reported by Woo *et al.* are in agreement with our claim that haploinsufficiency of CHCHD10 causes motoneuron degeneration. Additionally, our results from CHCHD10 knockdown in the vertebrate *in vivo* model confirm haploinsufficiency as the molecular basis of CHCHD10-linked neurodegeneration. It remains to be determined, if CHCHD10 mutations other than p.R15L and p.G66V also result in a loss of expression of the mutated protein, or if additional mechanisms are involved. The fact, that overexpression of CHCHD10^{R15L} leads to a phenotype as reported before (9) underlines the importance of expression studies in

patient-derived biomaterial: Cellular pathology upon overexpression of a mutant protein does not necessarily reflect a disease-relevant consequence of the mutation, in particular when studies in human biomaterial reveal that the respective mutant protein is most likely not expressed in patients.

The results presented here are critically relevant for the design of future studies to elucidate CHCHD10-related mechanisms of neurotoxicity and motoneuron degeneration in general. While the largest proportion of experimental work on CHCHD10 mutations is based on overexpression systems to date (3,7,9), our data suggest the validity of knockdown paradigms, at least for the two pathogenic mutations analysed in this study. Our findings furthermore underline the critical importance to assess expression also of missense mutations in patient-derived biomaterial before further experimental work-up. Finally, we established an *in vivo* vertebrate model for CHCHD10-associated disorders that may help assessing novel treatment strategies.

Materials and Methods

Ethics statement

Informed written consent was obtained from all individuals donating cells for this study that was approved by the ethical review board according to the Declaration of Helsinki (WMA, 1964).

Cell culture

Human lymphoblastoid cell lines (LCLs) transformed with Epstein Barr Virus (16), primary fibroblasts and HEK293 cells were cultured under standard conditions (37° C, 5% CO₂) in the respective media (LCLs: RPMI with 10% FCS, Glutamax and

Penicillin/Streptavidin; Fibroblasts: RPMI with 10% FCS, Glutamax, 2.5 mM sodium pyruvate, Uridine, Amphotericin B and Gentamicin; HEK293: DMEM with 10% FCS) HEK293 cells were transfected using calcium phosphate co-precipitation as previously described (17) with minor modifications.

Quantitative real-time PCR, cDNA and genomic DNA sequencing

Total RNA was isolated from human LCLs and primary fibroblasts using the RNeasy Plus Mini Kit (QIAGEN; Hilden, Germany). Reverse transcription was carried out with the iScript™ cDNA Synthesis Kit (Bio-Rad Laboratories, Inc.; Hercules, California). Quantitative PCRs were run on a CFX96 Real Time System (Bio-Rad Laboratories, Inc.; Hercules, California) using the iQ™ SYBR® Green Supermix (Bio-Rad Laboratories, Inc., Hercules; California). Oligonucleotides for qRT-PCRs are listed in [Supplementary Material, Table S4](#). Ct-values of CHCHD10 were normalized to TBP using 2^{-ΔΔCt}-method (18).

For cDNA sequencing, the coding sequence of CHCHD10 (426 bp) was amplified from cDNA with oligonucleotides 5'-CGGG GATCCATGCCTCGGGGAAGCCG-3' and 5'-CGGCTCGAGGGCAG GGAGCTCAGAC-3' using KAPA HiFi DNA Polymerase (Kapa Biosystems; Wilmington, Massachusetts) in GC buffer according to the manufacturer's protocol. Genomic DNA (gDNA) was isolated from cells using the DNeasy Blood & Tissue kit (QIAGEN; Hilden, Germany). For Sanger sequencing of isolated DNA, oligonucleotides 5'-CGGCTCGAGGGCAGGGAGCTCAGAC-3' and 5'-CGGGGATCCATGCCTCGGGGAAGCCG-3' (cDNA) or 5'-TGTAACACGACGGCCAGT-3' and 5'-CAGGAAACAGCTATGACC-3' (gDNA) were used.

Plasmids

The coding sequences of human wild-type and mutated CHCHD10 (NM_001301339.1) as well as zebrafish (*Danio rerio*) CHCHD10 (NM_200784.1) including a C-terminal myc- tag were cloned into BamHI and XhoI sites of the mammalian expression vector pCS2+ (RZPD; Tutzing, Germany).

For recombinant protein expression in *E. coli*, the human CHCHD10 coding sequence was cloned into pGEX-4-T1 (GE Healthcare; Boston, Massachusetts) using BamHI and XhoI sites to express N-terminally GST-tagged human CHCHD10 wild-type and mutants.

Antibodies used for Western blotting

Primary antibodies were anti-CHCHD10 (25671-1-AP; Proteintech Group, Inc; Rosemont, Illinois; 1: 2000), anti- Myc-Tag (9B11, #2276, Cell Signaling Technology, Inc; Danvers, Massachusetts; 1: 2000), anti-GAPDH (10494-1-AP; Proteintech Group, Inc; Rosemont, Illinois; 1: 10 000) or anti-HSP60 (SPC-105, StressMarq; Cadboro Bay, Canada; 1: 1000), respectively. Secondary antibodies were anti-mouse IgG (H + L) HRP conjugate (G-21040, Thermo Scientific™; Waltham, Massachusetts; 1: 2000) and anti-rabbit IgG (H + L) HRP conjugate (G-21234, Thermo Scientific™; Waltham, Massachusetts; 1: 2000).

Immunocytochemistry

Fibroblasts were grown on poly-D-lysine coated cover slips for 48 h. After washing with phosphate buffered saline (PBS) cells were fixed with 4% paraformaldehyde in PBS and permeabilized

using 0.1% Triton X-100 and 100 mM glycine in PBS for 10 min each. To block unspecific antibody binding cells were treated with 1.5% bovine serum albumin and 0.1% Tween-20 in PBS for 30 min. Anti-TDP-43 (#10782-2-AP, Proteintech Group, Inc; Rosemont, Illinois; 1: 500) and purified mouse anti-TIAR (#610352, BD Laboratories, San Jose, California; 1: 500) as well as goat anti-Mouse IgG (H + L) Cross-Adsorbed secondary antibody, Alexa Fluor 647 and donkey anti-rabbit IgG (H + L) Highly Cross-Adsorbed secondary antibody, Alexa Fluor 488 (#A-21235 and #A-21206, Thermo Scientific™; Waltham, Massachusetts; 1: 750) were used as primary and secondary antibodies, respectively. Antibody incubation steps were performed for 1 h each. Finally, cells were washed with PBS and mounted using DAPI Fluoromount-G® Mounting Medium (Southern Biotech; Birmingham, Alabama).

Protein purification and CD spectroscopy

Cultures of *E. coli* BL21(DE3)pLysS (Merck KGaA; Darmstadt, Germany) transformed with pGEX-4-T1 CHCHD10 wild-type or mutants were induced with 0.1 mM IPTG at an OD₆₀₀ of 0.6–0.8. Protein expression was carried out at room temperature for 4 h. Recombinant proteins were purified using Glutathione Sepharose 4B (GE Healthcare; Boston, Massachusetts) according to the manufacturer's instructions. Subsequently, the GST-tag was cleaved using thrombin (GE Healthcare; Boston, Massachusetts) overnight at 4°C. After cleavage, thrombin was removed using p-Amino-benzamidine-agarose (Sigma-Aldrich Co. LLC; St. Louis, Missouri). Circular dichroism (CD) spectroscopy was performed in PBS with addition of 0.02% or 0.1% dodecylphosphocholine (DPC) in a Chirascan™ CD Spectrometer (Applied Photophysics Ltd; Leatherhead, United Kingdom).

Zebrafish care and procedures

Adult zebrafish (*Danio rerio*) were bred and maintained as previously described (19). Morpholino-modified antisense oligonucleotides (MO, morpholino) directed either against the translation initiation site (MO1; 5'-GACTGGACTTCTCTTGCCATTTC-3'; 100 μM) or a splice junction site (MO2 splice junction: exon1-intron1; 5'-CTACTGCATCTAAAGATACCTCGCT-3'; 300 μM) of zebrafish CHCHD10 were injected into fertilized wild-type zebrafish oocytes in the one cell stage using a FemtoJet microinjector (Eppendorf AG; Hamburg, Germany). A Morpholino Standard Control oligo (CoMO; 5'-CCTCTTACCTCAGTTACAATTTATA-3'; 300 μM) was used as control. All MOs were obtained from Gene Tools, LLC (Philomath, Oregon) and were solved in 200 mM potassium chloride.

For rescue experiments, capped sense mRNA was *in vitro* transcribed from pCS2+ plasmid coding for C-terminally myc-tagged zebrafish CHCHD10 using the mMESSAGE mMACHINE SP6 Transcription Kit (Thermo Scientific™; Waltham, Massachusetts) and coinjected (200 ng/μl in 200 mM potassium chloride) with MO2.

'Flight response and birefringence were measured at 48 h post fertilization (hpf) and 72 hpf, respectively, as previously described (20). To inhibit pigmentation, embryos were treated with 0.003% 1-phenyl-2-thiourea prior to microscopic analysis. For motoneuron stainings embryos were fixed at 48 hpf with Dent's fixative (4: 1 MeOH/DMSO) overnight at room temperature, rehydrated with MeOH/PBT (PBS + 0.1% Tween-20) in three steps with 20 min each and unspecific binding sites were blocked using 10% FCS in PBT (90 min at room temperature). Motoneurons of prepared

embryos were stained with SV2 antibody (Developmental Studies Hybridoma Bank; Iowa City, Iowa; 1: 100) and secondarily with anti-mouse IgG (H + L) DyLight 488 conjugate (#35502, Thermo Scientific™; Waltham, Massachusetts; 1: 500). Each antibody staining step was performed for 2 days at 4° C. Confocal microscopy was carried out with a confocal laser scanning microscope (Leica TCS SP8) and motoneuron axon length was determined using ImageJ software (21).

Transmission electron microscopy

For transmission electron microscopy (TEM), patient-derived cells were kept on carbon-coated sapphire discs for at least 48 h. LCLs were prefixed using 0.1% glutaraldehyde, 4% paraformaldehyde and 1% saccharose in 0.1 M phosphate buffer (pH7.3). After high-pressure freezing cells were freeze-substituted with 0.2% osmium tetroxide, 0.1% uranyl acetate and 5% of water in acetone (22) and embedded in epon. Fibroblasts were high-pressure frozen without prefixation and freeze-substituted as described above. Zebrafish embryos at 48 hpf were fixed with 2.5% glutaraldehyde, post-fixed in 2% osmium tetroxide and dehydrated using a stepwise increase of isopropanol concentration, contrasted with uranyl acetate and embedded in epon. Images of ultrathin sections (80 nm) were taken using a JEOL JEM-1400.

Mass spectrometry

Sample preparation

Zebrafish embryos were lysed by addition of lysis buffer containing 6 M guanidine hydrochloride, 10 mM TCEP [Tris(2-carboxyethyl)phosphine hydrochloride], 40 mM 2-chloroacetamide and 100 mM triethylammonium bicarbonate (TEAB) followed by sonication and heating at 90° C for 5 min. The lysates were centrifuged at 10 000 × g for 30 min at 4° C and the supernatant was collected for further analysis. Protein concentration was determined using the Pierce™ BCA Protein Assay Kit (Thermo Scientific™; Waltham, Massachusetts).

Protein digestion was performed with a filter-aided sample preparation (FASP) protocol. In brief, the lysates were buffer exchanged with 50 mM TEAB (4×) using a Microcon-30 kDa centrifugal filter (Merck Chemicals GmbH; Darmstadt, Germany) and concentrated on the filter. 50 µl of trypsin/LysC (Promega; Madison, Wisconsin) in 50 mM TEAB were added to a final protein-to-enzyme ratio of 50: 1. Digestion was performed for 16 h at 37° C and 600 rpm. The resulting peptides were centrifuged through the filter and centrifugation was repeated after addition of 50 µl 0.2% TFA to increase recovery. Both flow throughs were pooled and peptide concentration was determined by absorption at 280 nm.

Label-free quantification of CHCHD10 by parallel reaction monitoring

From each sample, 2 µg of digested peptides were adjusted to a volume of 10 µl with 0.5% TFA and 5 µl (1 µg) were injected. The peptides were separated on a 20×0.075 mm, 3 µm trap column (Thermo Scientific™; Waltham, Massachusetts; PepMap100 C18) and a PepMap100 C18, 500×0.050 mm, 2 µm analytical column (Thermo Scientific™; Waltham, Massachusetts) with a column temperature of 60° C using a Dionex Ultimate3000 RSLCnano system (Thermo Scientific™; Waltham, Massachusetts). Mobile phase of the loading pump (trap column) was 0.05% TFA/2% MeOH (flow rate: 5 µl/min). The mobile phase of the nano pump (analytical column) was A: 4% DMSO/0.1% formic acid and B: 4% DMSO/76% acetonitrile/0.1% formic acid and peptides were eluted

with a linear gradient from 1% B to 53% in 21 min (flow rate: 150 nl/min) and infused into a Thermo QExactive mass spectrometer (MS). The MS was run in targeted MS²-mode (positive) with a resolution of 35 000, NCE 25, isolation window 1.6 m/z, AGC target 3e6 and max injection time of 128 ms.

For CHCHD10 determination (UniProtID Q6PBP6), parallel reaction monitoring (PRM) was performed for the peptide LPPSQSGPCLFEVR (aa95–108, precursor mass: m/z 793.9) and the y12 (m/z 1376.6627) and y13²⁺ (m/z 737.3614) fragments (deviation < 5ppm) were used for label-free quantification with Skyline 3.6 (23).

Proteomic analysis of zebrafish embryos

The digested peptides from each sample were diluted 1: 1 with 2% TFA and fractionated by strong cation exchange (Sigma-Aldrich Co. LLC; St. Louis, Missouri; #66889-U) using STAGE Tips. Peptides were eluted using 160 mM ammonium acetate/20% acetonitrile/0.5% formic acid (fraction 1), 300mM ammonium acetate/20% acetonitrile/0.5% formic acid (fraction 2) and 5% ammonium hydroxide/80% acetonitrile (fraction 3). The three fractions were vacuum dried and redissolved in 12 µl 0.5% TFA. Peptide concentration was determined by absorption at 280 nm.

From each fraction, 2 µg of peptides were injected using the same instrument configuration and mobile phases as described for the PRM. The peptides were separated with a two-step and three-step linear gradient: fraction 1: 1% B to 20% B from 5 to 120 min, 20% B to 53% B from 120 to 145 min, fraction 2: 1% B to 32% B from 5 to 120 min, 32% B to 53% B from 120 to 145 min, fraction 3: 1% B to 10% B from 5 to 20 min, 10% B to 32% B from 20 to 120 min, 32% B to 53% B from 120 to 145 min. Data were acquired by data-dependent acquisition (Top15) with the following settings: full MS: resolution 70 000, AGC target 3e6, max injection time 120 ms, scan range 400–1400 m/z, MS²: resolution 17 500, AGC target 1e6, max injection time 65 ms, isolation window 1.6 m/z, NCE 25 and a dynamic exclusion of 40 s.

Proteins were identified using MaxQuant 1.5.2.8 (24) and the *Danio rerio* reference proteome from UniProt (downloaded 04 February 2017). Trypsin without cleavage before proline was set as the enzyme allowing up to two missed cleavages, N-terminal acetylation and methionine oxidation were set as variable modifications and carbamidomethylation on cysteine residues as fixed modification. A FDR of 1% was used for peptide and protein identification and protein quantification was performed with the MaxLFQ algorithm (25). Quantitative analysis of the data was performed with Perseus 1.5.2.6 (26). Contaminant proteins and proteins identified with < 2 unique peptides were excluded.

Statistical analysis

In total, 7132 proteins were detected and 6116 proteins quantified in all samples were considered. Proteins showing minimal variations (fold change < ± 1.5) between the different conditions were excluded from the analysis. Proteins with a fold change ≥ ± 1.5 were retained. A two-tailed student's t-test was used to identify differentially expressed proteins between the groups and p-values were corrected for multiple testing using FDR-correction. FDR-values ≤ 0.05 were considered statistically significant. Hierarchical cluster analysis was performed using the Genesis software package (27).

Supplementary Material

Supplementary Material is available at HMG online.

Acknowledgements

We are indebted to the patients and their families for their participation in this project. Further, we appreciate the excellent technical assistance of Elena Jasovski, Aline Sage, Nadine Todt, Jessica Rudloff and the teams of the Core Facilities for Electron Microscopy and Confocal Microscopy at Ulm University.

Conflict of Interest statement. None declared.

Funding

This work was supported in whole or in parts by a grant from the German Federal Ministry of Education and Research (JPND "STRENGTH" consortium; German network for ALS research MND-NET) [BMBF 01ED1408]; the German Society for patients with muscular diseases (DGM) [We 6/1]; and the International Graduate School in Molecular Medicine Ulm funded by the Excellence Initiative of the German Federal and State Governments [GCS 270].

References

- Polymenidou, M. and Cleveland, D.W. (2008) Motor neuron disease: The curious ways of ALS. *Nature*, **454**, 284–285.
- Carri, M.T., D'Ambrosi, N. and Cozzolino, M. (2017) Pathways to mitochondrial dysfunction in ALS pathogenesis. *Biochem. Biophys. Res. Commun.*, **483**, 1187–1193.
- Bannwarth, S., Ait-El-Mkadem, S., Chausse, A., Genin, E.C., Lacas-Gervais, S., Fragaki, K., Berg-Alonso, L., Kageyama, Y., Serre, V. and Moore, D.G. (2014) A mitochondrial origin for frontotemporal dementia and amyotrophic lateral sclerosis through CHCHD10 involvement. *Brain*, **137**, 2329–2345.
- Muller, K., Andersen, P.M., Hubers, A., Marroquin, N., Volk, A.E., Danzer, K.M., Meitinger, T., Ludolph, A.C., Strom, T.M. and Weishaupt, J.H. (2014) Two novel mutations in conserved codons indicate that CHCHD10 is a gene associated with motor neuron disease. *Brain*, **137**, e309.
- Penttilä, S., Jokela, M., Saukkonen, A.M., Toivanen, J., Palmio, J., Lahdesmaki, J., Sandell, S., Shcherbii, M., Auranen, M., Ylikallio, E. et al. (2017) CHCHD10 mutations and motor neuron disease: the distribution in Finnish patients. *J. Neurol. Neurosurg. Psychiatry*, **88**, 272–277.
- Jokela, M., Penttilä, S., Huovinen, S., Hackman, P., Saukkonen, A.M., Toivanen, J. and Udd, B. (2011) Late-onset lower motor neuronopathy A new autosomal dominant disorder. *Neurology*, **77**, 334–340.
- Genin, E.C., Plutino, M., Bannwarth, S., Villa, E., Cisneros-Barroso, E., Roy, M., Ortega-Vila, B., Fragaki, K., Lespinasse, F., Pinero-Martos, E. et al. (2016) CHCHD10 mutations promote loss of mitochondrial cristae junctions with impaired mitochondrial genome maintenance and inhibition of apoptosis. *EMBO Mol. Med.*, **8**, 58–72.
- Jokela, M., Huovinen, S., Raheem, O., Lindfors, M., Palmio, J., Penttilä, S., Udd, B. and Wishart, T.M. (2016) Distinct muscle biopsy findings in genetically defined adult-onset motor neuron disorders. *PLoS One*, **11**, e0151376.
- Woo, J.-A.A., Liu, T., Trotter, C., Fang, C.C., De Narvaez, E., LePochat, P., Maslar, D., Bukhari, A., Zhao, X., Deonaraine, A., Westerheide, S.D. and Kang, D.E. (2017) Loss of function CHCHD10 mutations in cytoplasmic TDP-43 accumulation and synaptic integrity. *Nat. Commun.*, **8**, 15558.
- Kurzweil, D., Kruger, S., Biskup, S. and Heneka, M.T. (2015) A distinct clinical phenotype in a German kindred with motor neuron disease carrying a CHCHD10 mutation. *Brain*, **138**, e376.
- Johnson, J.O., Glynn, S.M., Gibbs, R., Nalls, M.A., Sabatelli, M., Restagno, G., Drory, V.E., Chio, A., Rogaeva, E. and Traynor, B.J. (2014) Mutations in the CHCHD10 gene are a common cause of familial amyotrophic lateral sclerosis. *Brain*, **137**, e311.
- Marroquin, N., Stranz, S., Muller, K., Wieland, T., Ruf, W.P., Brockmann, S.J., Danzer, K.M., Borck, G., Hubers, A. and Weydt, P. (2015) Screening for CHCHD10 mutations in a large cohort of sporadic ALS patients: no evidence for pathogenicity of the p.P34S variant. *Brain*, **139**, e8.
- Wong, C.H., Topp, S., Gkazi, A.S., Troakes, C., Miller, J.W., de Majo, M., Kirby, J., Shaw, P.J., Morrison, K.E., de Belleruche, J. et al. (2015) The CHCHD10 P34S variant is not associated with ALS in a UK cohort of familial and sporadic patients. *Neurobiol. Aging*, **36**, 2908 e2917–e2908.
- Kurosaki, T. and Maquat, L.E. (2016) Nonsense-mediated mRNA decay in humans at a glance. *J. Cell Sci.*, **129**, 461–467.
- Straub, I.R., Janer, A., Weraarpachai, W., Zinman, L., Robertson, J., Rogaeva, E. and Shoubridge, E.A. (2017) Loss of CHCHD10-CHCHD2 complexes required for respiration underlies the pathogenicity of a CHCHD10 mutation in ALS. *Hum. Mol. Genet.*, **27**, 178–189.
- Ventura, M., Gibaud, A., Le Pendu, J., Hillaire, D., Gérard, G., Vitrac, D. and Oriol, R. (1988) Use of a simple method for the Epstein-Barr virus transformation of lymphocytes from members of large families of Réunion Island. *Hum. Hered.*, **38**, 36–43.
- Jordan, M. and Wurm, F. (2004) Transfection of adherent and suspended cells by calcium phosphate. *Methods*, **33**, 136–143.
- Livak, K.J. and Schmittgen, T.D. (2001) Analysis of relative gene expression data using real-time quantitative PCR and the 2^{-ΔΔC_T} method. *Methods*, **25**, 402–408.
- Just, S., Meder, B., Berger, I.M., Etard, C., Trano, N., Patzel, E., Hassel, D., Marquart, S., Dahme, T., Vogel, B. et al. (2011) The myosin-interacting protein SMYD1 is essential for sarcomere organization. *J. Cell Sci.*, **124**, 3127–3136.
- Buhrdel, J.B., Hirth, S., Kessler, M., Westphal, S., Forster, M., Manta, L., Wiche, G., Schoser, B., Schessl, J., Schroder, R. et al. (2015) In vivo characterization of human myofibrillar myopathy genes in zebrafish. *Biochem. Biophys. Res. Commun.*, **461**, 217–223.
- Schneider, C.A., Rasband, W.S. and Eliceiri, K.W. (2012) NIH Image to ImageJ: 25 years of image analysis. *Nat. Methods*, **9**, 671–675.
- Buser, C. and Walther, P. (2008) Freeze-substitution: the addition of water to polar solvents enhances the retention of structure and acts at temperatures around -60 degrees C. *J. Microsc.*, **230**, 268–277.
- MacLean, B., Tomazela, D.M., Shulman, N., Chambers, M., Finney, G.L., Frewen, B., Kern, R., Tabb, D.L., Liebner, D.C. and MacCoss, M.J. (2010) Skyline: an open source document editor for creating and analyzing targeted proteomics experiments. *Bioinformatics*, **26**, 966–968.
- Cox, J. and Mann, M. (2008) MaxQuant enables high peptide identification rates, individualized p.p.b.-range mass accuracies and proteome-wide protein quantification. *Nat. Biotechnol.*, **26**, 1367–1372.

25. Cox, J., Hein, M.Y., Lubner, C.A., Paron, I., Nagaraj, N. and Mann, M. (2014) Accurate proteome-wide label-free quantification by delayed normalization and maximal peptide ratio extraction, termed MaxLFQ. *Mol. Cell. Proteomics*, **13**, 2513–2526.
26. Tyanova, S., Temu, T., Sinitcyn, P., Carlson, A., Hein, M.Y., Geiger, T., Mann, M. and Cox, J. (2016) The Perseus computational platform for comprehensive analysis of (prote)omics data. *Nat. Methods*, **13**, 731–740.
27. Sturn, A., Quackenbush, J. and Trajanoski, Z. (2002) Genesis: cluster analysis of microarray data. *Bioinformatics*, **18**, 207–208.
28. The UniProt Consortium. (2017) UniProt: the universal protein knowledgebase. *Nucleic Acids Res*, **15**, D158–D169.